# Multiscale Simulation of Soft Matter: From Scale Bridging to Adaptive Resolution

Matej Praprotnik,* Luigi Delle Site, and Kurt Kremer

Max-Planck-Institut für Polymerforschung, D-55128 Mainz, Germany; email: praprot@mpip-mainz.mpg.de, dellsite@mpip-mainz.mpg.de, kremer@mpip-mainz.mpg.de

Annu. Rev. Phys. Chem. 2008. 59:545–71

First published online as a Review in Advance on December 6, 2007

The *Annual Review of Physical Chemistry* is online at http://physchem.annualreviews.org

This article's doi: 10.1146/annurev.physchem.59.032607.093707



0066-426X/08/0505-0545$20.00

* On leave from the National Institute of Chemistry, Ljubljana, Slovenia.

## Key Words

multiscale modeling, generalized equipartition theorem, atomistic simulation, mesoscopic simulation

## Abstract

The relation between atomistic chemical structure, molecular architecture, molecular weight, and material properties is of basic concern in modern soft material science and includes standard properties of bulk materials and surface and interface aspects, as well as the relation between structure and function in nanoscopic objects and molecular assemblies of both synthetic and biological origin. This all implies a thorough understanding on many length and correspondingly time scales, ranging from (sub)atomistic to macroscopic. Presently, computer simulations play an increasingly important, if not central, role. Some problems do not require specific atomistic details, whereas others require them only locally. However, in many cases this strict separation is not sufficient for a comprehensive understanding of systems, and flexible simulation schemes are required that link the different levels of resolution. We here give a general view of the problem regarding soft matter and discuss some specific examples of linked simulation techniques at different resolution levels. We then discuss a recently developed flexible simulation scheme, the AdResS method, which allows one to adaptively change the resolution in certain regions of space on demand.

## 1. INTRODUCTION

Synthetic and biological macromolecules, (bio)membranes, colloidal suspensions, and so on are classified under the general term soft matter. The term soft in this context means that the characteristic energy densities, which to a first approximation are close to the elastic constants, are several orders of magnitude smaller than for conventional hard matter. The relevant energy scale is the thermal energy $k_BT$, approximately $4.1 \times 10^{-21}$ J at room temperature. This goes in hand with large fluctuations; in other words, the conformational entropy of a macromolecule is of the same order as the intermolecular energy, and the interplay among them usually determines the relevant properties.

Macromolecules or polymers are huge molecules of a wide variety of architecture and nature. They are built from identical or a few building blocks that are connected into long chain molecules or structures of a more complicated topology. The conceptually most simple case comprises long chain molecules of identical repeat units. More complicated objects are starlike polymers or polymer networks and gels. Combining several different synthetic or biological building blocks leads to copolymers. Thus one can view proteins as an especially interesting and challenging example of multiblock copolymers.

Macromolecules have been extensively studied on the basis of rather simple generic models. These ideas date back to the seminal work of Flory (1, 2) and others and the subsequent solid theoretical basis and link to critical phenomena are from de Gennes (3), who showed that all polymers follow the same universal scaling laws and that one can understand qualitatively and semiquantitatively their behavior on the basis of scaling theories [i.e., the mean squared extension of a polymer, $R^2(N)$, follows the scaling law $\langle R^2(N)\rangle = AN^{2\nu}$, where $\nu$ is a universal critical exponent]. In so-called good solvent $\nu \simeq 0.6 (d = 3)$, whereas it is 1/2 in a polymer melt. Although the power law is universal, scaling theory says nothing about the prefactor $A$, which is determined by the polymer's chemical structure and its interaction with its surroundings and can vary significantly. Similar relations hold for many other properties, including dynamics (3, 4). For quantitative material properties, both are equally important. With regard to mixtures, molecular assemblies, functional systems, and so on, one usually does not fully reach the scaling regime, and the combination of generic and chemistry-specific information is absolutely conditional for any theoretical prediction. **Figure 1** illustrates the different scales and characteristic means of investigation by computer simulations.

As illustrated above in a simple example, many phenomena in biology, chemistry, and materials science involve processes occurring on atomistic length and time scales that affect structural and dynamical properties on mesoscopic scales exceeding far beyond atomistic ones. Because it is infeasible (and most often undesirable) to run computer simulations of very large systems with atomistically detailed models, mesoscale (coarse-grained) models are being developed through which structural relaxations can be studied at large length scales, allowing for full system equilibration on mesoscopic time scales (5). Ideally, these coarse-grained (CG) models stay reasonably close to the chemical structure of the material, so the reintroduction of chemical

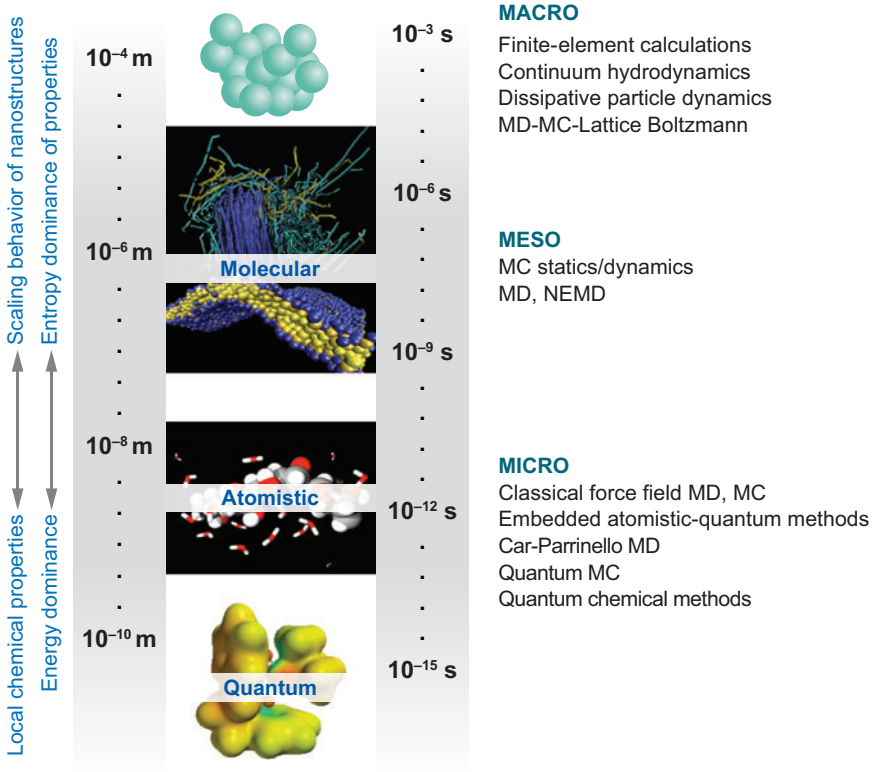


**Figure 1**

Illustration of the different length and time scales relevant for the simulation of soft matter. Here we deal with the lower three levels of resolution, which all introduce features that carry through into the macroscopic properties of the systems. We show only a selection of representative methods employed at each scale. MC, Monte Carlo; MD, molecular dynamics; NEMD, nonequilibrium molecular dynamics.

details allows the study of atomistically detailed processes in various windows of the CG trajectory (6–10). With such a methodology at hand, one can use CG models to describe chemically realistic systems over a wide range of length and time scales in a hierarchical, sequential set of simulations at multiple resolution levels, or in a single, multiscale simulation in which the resolution level can be changed at will, locally or adaptively (in the course of a simulation). This linking requires the (high- and low-) resolution models to be (pairwise) structurally consistent. Because many high-resolution states correspond to a specific lower-resolution state, the conformational statistics on both resolution levels should be the same if analyzed on the CG level.

In this article, we emphasize a structure-based coarse graining with the aim to allow for structure-based scale hopping (11). On this basis we then discuss an adaptive resolution scheme, which allows us to zoom in/out on the fly in a certain subregion of the system, maintaining true equilibrium between a CG and a more detailed atomistic

region (12–14). In doing so, we follow a coarse-graining prescription without using ad hoc input to obtain the desired properties in a correct way. Alternative coarse-graining approaches (15–17), as well as approaches that go much further and map the whole chain to one ellipsoidal particle (18, 19) or just a soft sphere (20), are not discussed here. For a general overview of advanced computer simulation techniques, we refer the reader to References 21 and 22.

## 2. MULTISCALE MODELING OF SOFT MATTER

In this section we discuss coarse graining for the specific example of bisphenol-A polycarbonate (BPA-PC) in bulk and close to a metal surface. For this, we first introduce the structure-based coarse-graining approach.

### 2.1. Structure-Based Coarse-Graining Approach

The structure-based coarse-graining approach begins with the mapping scheme, which has both the task of simplifying the interactions as much as possible and the task of staying close to the chemical structure to allow for scale hopping (6, 7, 10, 11) up and down. **Figure 2*a*** gives an example of how this is done for BPA-PC, in which the mapping points are the centers of the carbonate and isopropylene groups, and a sphere for the benzene rings is added along the connection line between these points.[1]

To generate the interaction potentials for the CG system, we strictly separate the parameterization of bonded and nonbonded interactions and derive them independently. This makes the CG models transferable, at least in part, from one situation to another. Based on the assumption that the total potential energy can be separated into a bonded/covalent ($U_B^{cg}$) and nonbonded ($U_{NB}^{cg}$) contribution, we derive $U_B^{cg}$ for the CG bond and torsion angles and bond lengths by sampling distribution functions of the underlying atomistic model in vacuum either by Monte Carlo or molecular dynamics (MD) with a stochastic thermostat. Because any double counting of interactions with respect to the later treated nonbonded interactions has to be avoided, correlations along the backbone are only considered up to the distance needed to generate the appropriate distributions. The underlying atomistic potentials are determined preferably by quantum calculations and thus are not linked to any parameterization based on experiment or other simulations, which typically include already further interactions. The distributions in general are characterized by the CG bond lengths $r$, bond angles $\theta$, and torsions $\phi$ [i.e., $P(r, \theta, \phi, T)$]. Note that in many cases one has to consider several different bond and torsion angles (e.g., for BPA-PC, two bond angles at the isopropylidene and carbonate group, $\theta_1$ and $\theta_2$), whereas one torsion potential around the carbonate junction is sufficient. For simplicity, we assume that $P(r, \theta_1, \theta_2, \phi, T) = P(r, T)P(\theta_1, T)P(\theta_2, T)P(\phi, T)$ factorizes. This assumption generally does not hold, and the introduced error strongly depends on the details

[1]An earlier version that included the benzenes in the other two spheres (6, 7, 9) resulted in very similar structures; however, it turned out to be rather inefficient owing to caging effects. For general discussion of this point, we refer the reader to Reference 10.

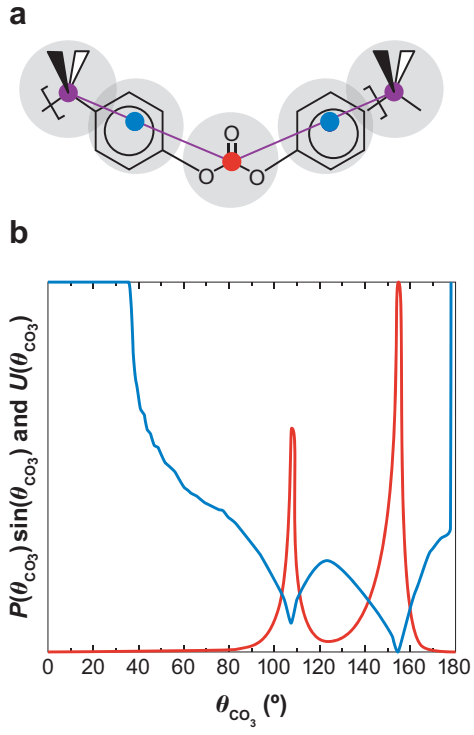


**Figure 2**

(*a*) Mapping scheme for bisphenol-A polycarbonate. (*b*) Distribution of $\theta_{CO_3}$ (*red*) and the corresponding effective potential (*blue*) at the process temperature of 570 K.

of the chosen CG model (23). For BPA-PC the two bond angles trivially decouple, and the torsion potential is flat, so the above requirement is fulfilled to a good approximation. Boltzmann inversion of the distributions yields temperature-dependent bonded CG interaction potentials:

$$U^{cg}(r, T) = -k_B T \ln[P(r, T)/r^2] + const_r, \quad (1)$$

$$U^{cg}(\theta_i, T) = -k_B T \ln[P(\theta_i, T)/\sin\theta_i] + const_{\theta_i}, \quad (2)$$

$$U^{cg}(\phi, T) = -k_B T \ln[P(\phi, T)] + const_\phi. \quad (3)$$

**Figure 2*b*** shows a typical example for the bond angle $\theta$ at the carbonate group of BPA-PC. The temperature dependence concerns not only the prefactor $k_BT$, but also the distributions $P$ themselves. Strictly speaking they can only be applied at the temperature at which they were derived.

One can introduce the nonbonded interactions by matching the CG radial distribution functions of small all-atom chains under the appropriate melt or solution conditions. An example of a typical procedure leading to the appropriate tabulated potential is the iterative Boltzmann inversion method (16, 24). For apolar, amorphous polymers, a more direct and simpler approach is usually sufficient. The excluded

volume of the CG beads is given by repulsive short-range potentials in which the parameters are either estimated by group contribution methods or from the van der Waals volumes of the beads. For BPA-PC the latter was sufficient, leading to simple repulsive Lennard-Jones potentials (Weeks-Chandler-Andersen potential) (25). To set up the initial melt conformations, we follow Auhl et al.'s (26) procedure, which has been applied to a number of different CG models and has been shown to be robust and efficient. Using this approach, investigators have successfully studied a variety of polymer melts. With this procedure, we find for BPA-PC a characteristic ratio $\langle R_G^2 \rangle / N \approx 37$ Å$^2$, where $R_G$ is the radius of gyration and $N$ is the number of repeat units. This compares well to neutron-scattering experiments (9) and allowed us to study structural as well as dynamic properties of BPA-PC melts for systems up to 200 chains and up to 20 entanglement molecular weights ($N_e \approx 5 - 6$, $N = 120$), corresponding to system sizes of (100 nm)$^3$ (27, 28).

## 2.2. Inverse Mapping

The above section gives a short account of the coarse-graining procedure we usually employ for amorphous polymers. As mentioned, however, the whole setup is still close to the chemical structure of the backbone. This should allow us to reintroduce the chemical details of the chains and by that allow for a detailed comparison to microscopic experiments and also, if successful, allow for the anticipated scale hopping or adaptive resolution simulation. There are several options for the reintroduction of chemical details (6, 7, 11, 25, 28, 29). If the polymers consist of reasonably rigid (all-atom) fragments, it is sufficient to fit these rigid all-atom units onto the corresponding CG chain-segment coordinates. The atomistic fragments are taken from a pool of structures that correctly reflect the statistical weight of those degrees of freedom (DOFs) (i.e., ring flips) that are not resolved in the CG description. Then a short equilibration run of a few picoseconds is performed. In the case of BPA-PC, the typical distance individual atoms moved during this short equilibration was below 1.5 Å. Taking the size of one monomer, the carbonate-carbonate distance is approximately 11 Å; this is just a very local rattling. The derived structures compare well to scattering experiments (**Figure 3*a***) (28).

Together with the characteristic ratio, the scattering function indicates that the obtained all-atom melts truly represent the experimental system, supporting the overall consistency of the approach. Note that this procedure does not require any fitting to experiment for the bonded part and, for the present case, not even for the nonbonded part. In the first application for phenol diffusion in BPA-PC (30), the polymer matrix was generated by the above procedure to host the added small molecules.

This whole procedure has also become an important tool for studying polymer dynamics (27, 28). Although the length scaling is obvious from the mapping procedure, this is more complex for dynamics. The CG units of $\varepsilon$, $\sigma$, and $\tau$ (the typical Lennard-Jones units) define a natural time scale. This, however, is the physical time only up to a system-dependent prefactor. The motion of the chains is mostly governed by the bead friction owing to local packing and chain connectivity. One way to resolve this is to match mean square displacements of a short chain atomistic melt

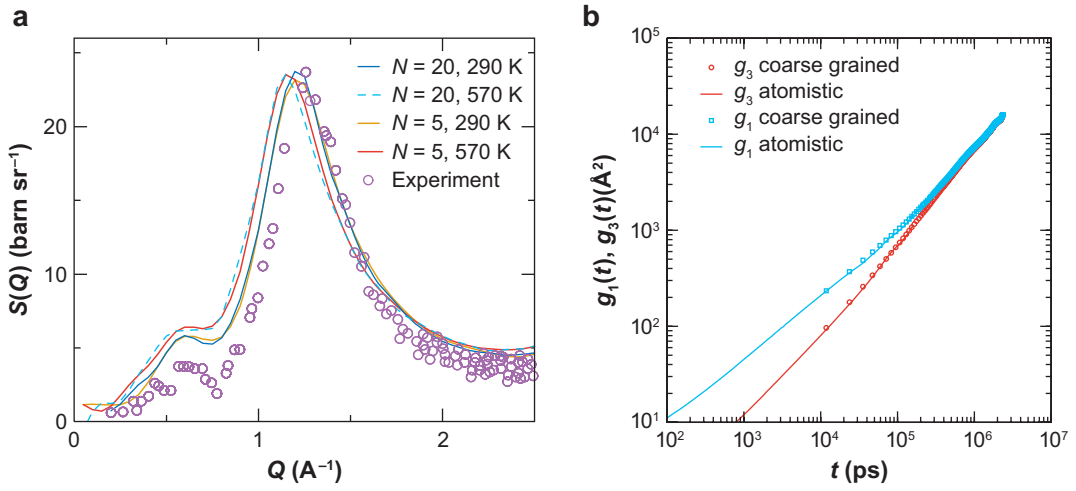


**Figure 3**

(*a*) Structure factor of a BPA-PC melt obtained by neutron scattering and from simulations after reinserting atomistic details at the temperatures indicated. (*b*) Chains' mean square displacement from atomistic and coarse-grained simulations to determine the time scaling for the coarse-grained simulations. Figure taken from Reference 28.

with those of a corresponding CG melt (see **Figure 3*b***). Doing this not only gives the time scaling but also shows down to what scale the CG description follows the appropriate molecular motion. In the case of BPA-PC at the typical process temperature of 570 K, we find that $1\tau \approx 30$ ps and that the CG displacements properly represent atomistic trajectories down to distances of approximately 10 Å, roughly the size of a monomer. Combining all this means that in our case we now have systems with approximately 800,000 atoms for times of up to $5 \times 10^{-4}$ s. Along these lines we also recently investigated a variety of problems related to polystyrene (23, 31).

## 2.3. Bisphenol-A Polycarbonate at a Metal Surface: Dual-Scale Approach

Whereas dispersion forces lead to an overall polymer attraction to the surface, the resulting changes of the melt conformations are well described by rather idealized theories. In the case of a metal surface, such as Ni, however, specific interactions of chain fragments might lead to rather different morphologies, as shown for the example of BPA-PC (32). In this example, the above CG scheme was combined with an ab initio density-functional MD study of specific surface interactions. For this, the investigators had to cut the monomer into pieces, and they studied the interaction of the submolecules benzene and phenol, carbonic acid, and propane with an Ni(1,1,1) surface (33). The quantum-mechanical calculations are restricted to those submolecular configurations that are allowed by the chain topology. Both carbonic acid and propane are strongly repelled by the Ni surface, starting at approximately

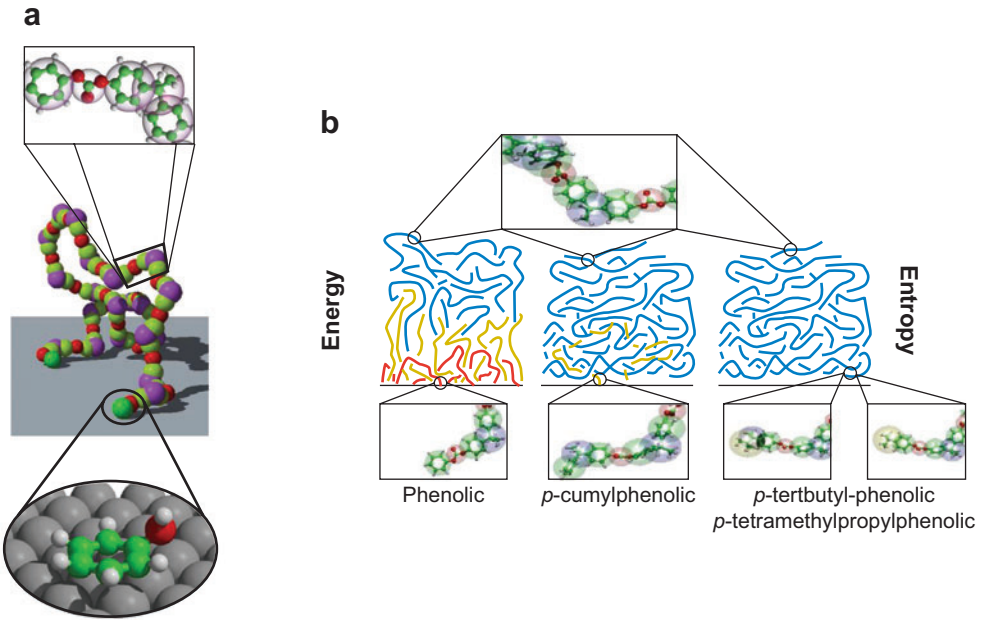


**Figure 4**

(*a*) Dual-scale model of BPA-PC on a nickel surface. (*b*) Entropy-energy interplay as illustrated by different chain ends. Figure adapted from Reference 33.

3 Å and reaching approximately 1.5 eV $\simeq$ 30 $k_BT$ at 570 K and 0.9 eV $\simeq$ 18 $k_BT$, respectively, at approximately 2 Å. In contrast, benzene and phenol are strongly attracted (1 eV $\simeq$ 20 $k_BT$) but at small distances (2 Å) only, requiring the benzene plane to lie flat on the surface owing to the overlap of the Ni and benzene $\pi$ electrons. This leads to a situation in which only the terminal benzenes can adsorb within a special local conformation, whereas benzenes within the chains are prevented from adsorption by the carbonate and the isopropylidene group. The latter requires a dual-scale approach (32) in which the angular potentials at the CG carbonate groups next to the terminal phenols are kept at the full atomistic resolution. **Figure 4** illustrates the outcome and the setup of the simulation.

The comparison of different chain ends shows that the melt morphology close to the surface for phenolic chain ends is significantly different from the generic dispersion force dominated structure (33). This has also been extended to study the sliding of BPA-PC melts under shear with and without additives (34–36) and at a surface defect (37).

This example illustrates that even within one simulation different resolution levels might be appropriate (e.g., see 15, 38–54). Because in this example the higher resolution was applied only to the chain ends, the computational costs are relatively small. Other cases, however, such as situations in which this applies to whole molecules, require strategies to adaptively change the resolution levels.

## 3. ADAPTIVE RESOLUTION SIMULATION

### 3.1. Motivations

The above section introduces a systematic coarse-graining procedure that allowed the efficient simulation of a system on a lower level of resolution while keeping the option of reintroducing the chemical details whenever needed. This methodology, however, applies to the whole system. Instead a highly desirable approach is one in which (two) levels of resolution can be applied at the same time within one simulation in different areas and in which both regimes are in true equilibrium with each other, allowing for a free exchange of molecules. Then one could run a simulation on a lower level of detail and zoom in on the fly, whenever something interesting is happening.

Theoretical methods employed to study such systems span from quantum-mechanical to macroscopic statistical approaches (32, 33, 38, 39, 55–57). However, the common feature, and limitation, of all these methods is that the regions or parts of the system treated at different resolution levels are fixed and do not allow for particle exchange. Recently, we proposed the particle-based adaptive resolution scheme (AdResS) (12) for hybrid all-atom/CG MD simulations that fulfills the above requirement. The basic idea of this approach leads to the generalization of the equipartition theorem to noninteger dimensions of the phase space (14).

### 3.2. Adaptive Resolution Scheme (AdResS)

In the following we briefly describe a simulation scheme, which will allow one to adaptively adjust the resolution locally on demand, while keeping the equilibrium within the whole system.

**A multiresolution model.** We consider a system of $N$ molecules in a volume $V$, modeled on a rather CG level, in which a higher (i.e., all-atom) resolution is needed in a certain subvolume $V_B$. Thus the number $n$ of DOFs per molecule is lower in the CG region $V_A$ and higher in the all-atom region $V_B$. For simplicity, we divide the simulation volume $V$ into two equally large slabs $A$ and $B$. This poses the problem of how to reach true thermodynamic equilibrium between the two regions, keeping the same structure on both sides, if analyzed at the CG level, however, now within one simulation. At this point we assume that for a state point $(\rho, T)$ it is generally possible to reduce the many-body potential of the higher-resolution representation into a dimensionally reduced effective potential (7, 16, 24, 58–61). (Note that the pressure in the previously discussed case is usually different in the different regimes.) However, treating one overall system with regions of different resolution requires special attention. To address this we visualize the free energy $F$ as a function of the position $x$ and formally divide the system into large-enough equal slabs, so $F(x)$ remains a truly extensive quantity of the slab (see **Figure 5**). The free energy is a thermodynamic potential; hence in thermodynamic equilibrium $F(x) = F_A$, constant in region $A$, and $F(x) = F_B$, constant in region $B$. In general $F_A \neq F_B$ because $F$ is

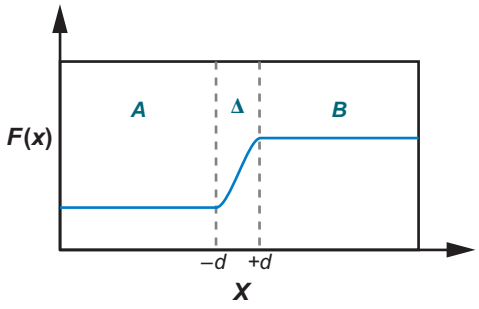


**Figure 5**

The free energy $F$ associated with DOFs explicitly considered in a simulation as a function of $x$. $A$ and $B$ are the regions with low and high levels of detail, respectively, whereas $\Delta$ is a transition regime. The constant values of $F_A$ and $F_B$ are arbitrary and do not play any role in the following treatment.

extensive and $n_A \neq n_B$. Despite this, the chemical potentials at the same molecular density must be equal in both regions. This guarantees that the molecules experience no spurious driving force into one region, keeping the liquid homogeneous across the box. From a molecular point of view, the artificial resolution boundary must be essentially invisible (i.e., the molecules have to cross the border without experiencing any barrier). Thus, at equilibrium, conditions analogous to two-phase coexistence,

$$\mu_A = \mu_B, \quad p_A = p_B, \quad T_A = T_B, \tag{4}$$

must be automatically satisfied, where $\mu_A$, $p_A$, and $T_A$ and $\mu_B$, $p_B$, and $T_B$ are the chemical potentials, pressures, and temperatures of the liquid in the CG and atomistic domains, respectively (12, 14). One can then view the part of the free energy associated with switching on and off DOFs as the equivalent of a latent heat per molecule, $q_l$.

To facilitate this, we introduce a transition regime $\Delta$ between the two subsystems (i.e., $-d \leq x \leq +d$; see **Figure 5**) of a minimal width set by the range of the effective pair potential between molecules in which the resolution gradually changes. Because the two regimes $A$ and $B$ are in equilibrium,

$$\left.\frac{\partial F_A(x)}{\partial x}\right|_{x\leq -d} = \left.\frac{\partial F_B(x)}{\partial x}\right|_{x\geq +d} = 0, \tag{5}$$

with $\frac{\partial F_A}{\partial x} = \frac{\partial F_A}{\partial N_A}\frac{\partial N_A}{\partial n_A}\frac{\partial n_A}{\partial x}$, similarly for $B$. $N_A$ and $N_B$ are the numbers of molecules in $A$ and $B$, respectively. Because $\partial N_A/\partial n_A$ and $\partial N_B/\partial n_B$ are nonzero and constant, and $\partial F_A/\partial N_A + q_l = \mu_A$ and $\partial F_B/\partial N_B = \mu_B$, this requires

$$\left.\frac{\partial n_A(x)}{\partial x}\right|_{x\leq -d} = \left.\frac{\partial n_B(x)}{\partial x}\right|_{x\geq +d} = 0 \tag{6}$$

in the regimes $A$ and $B$ (14). Consequently the weighting function $w(x)$, which interpolates between the two regimes by changing $n_{A,B}$ on the individual molecule level, has to have zero slope at the boundaries. For simplicity we choose $w(x)|_{x\leq -d} = 0$ and $w(x)|_{x\geq +d} = 1$, varying monotonically between 0 and 1. This has some formal

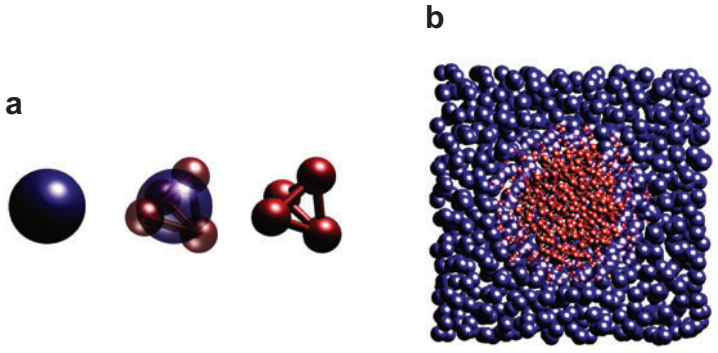


**Figure 6**

(*a*) The on-the-fly interchange between the atomistic (*far-right molecule*) and coarse-grained (*far-left molecule*) levels of description. The middle hybrid molecule is a linear combination of a fully atomistic molecule with an additional center-of-mass particle representing the coarse-grained molecule. (*b*) Snapshot of the hybrid atomistic/mesoscopic model liquid with $\rho = 0.175$ and $T = 1.0$. The red molecules are the explicit atomistically resolved tetrahedral molecules, and the blue molecules are the corresponding one-particle coarse-grained molecules.

similarities to the concept of phase equilibrium at a first-order phase transition. The switching function $w(x)$ plays the role of an order parameter, in which the transition is introduced by a geometrical constraint rather than the interactions. However, the fact that $F_A \neq F_B$ illustrates the limitations of the analogy above. In fact, in a phase transition the free energy at the transition point is the same in the two phases. Thus we have to devise a method that circumvents that problem in the transition regime $\Delta$.

**The AdResS method.** To smoothly couple the different regimes, we developed the AdResS method (12), which is a two-stage procedure. First, one has to define the CG sites/model and derive the effective pair potential $U^{cg}$ between CG molecules such that the statistical properties (i.e., the density, pressure, and temperature) of the corresponding all-atom system are accurately reproduced. For practical reasons, as shown below, it is also advisable to match the radial distribution functions as closely as possible.[2] To determine the interactions, one can follow the schemes discussed in the section above. Second, we introduce an interface layer (corresponding to the transition regime $\Delta$) between the atomistic and CG regions that contains hybrid molecules as illustrated in **Figure 6*a*** for the simple example of tetrahedral liquid molecules (12). There each hybrid molecule corresponds to an all-atom molecule with an additional massless center-of-mass particle serving as an interaction site. The transition is then governed by a weighting function $w(x) \in [0,\ 1]$ that interpolates the molecular interaction forces between the two regimes and assigns the identity of the molecule. $w(x)$ is defined in such a way that $w = 1$ corresponds to high resolution, $w$

[2]This actually allows one to easily zoom in on a CG simulation on the fly, wherever this is of interest.

$= 0$ to low resolution, and values $0 < w < 1$ to the transition regime. Interpolating forces and not potentials acting between the centers of mass of molecules $\alpha$ and $\beta$ (12) leads to

$$\mathbf{F}_{\alpha\beta} = w(x_\alpha)w(x_\beta)\mathbf{F}^{ex}_{\alpha\beta} + [1 - w(x_\alpha)w(x_\beta)]\mathbf{F}^{cg}_{\alpha\beta}, \tag{7}$$

where $\mathbf{F}_{\alpha\beta}$ is the total intermolecular force acting between the centers of mass of the molecules $\alpha$ and $\beta$, $\mathbf{F}^{ex}_{\alpha\beta}$ is the sum of all pair atom interactions between explicit atoms of the molecule $\alpha$ and explicit atoms of the molecule $\beta$, $\mathbf{F}^{cg}_{\alpha\beta} = -\nabla U^{cg}_{\alpha\beta}$ is the effective pair force between the two molecules, and $x_\alpha$ and $x_\beta$ are the $x$ center-of-mass coordinates of the molecules $\alpha$ and $\beta$, respectively. As given by Equation 7, AdResS by construction satisfies Newton's third law, among others crucial for the proper diffusion of molecules across the resolution boundaries (62). Because the total pair force as defined by Equation 7 depends not only on their relative distances but also on the absolute positions of the molecules, it is not conservative and the corresponding potential does not exist (63). The work done by this force depends on the physical path taken by the respective hybrid molecule in the transition regime (i.e., on the number of particle collisions encountered on the way). However, despite the fact that within the AdResS method we cannot define the free energy in the transition region, the grand-canonical potential $\Omega = -pV$ is nevertheless a well-defined and conserved quantity in our approach. Because Equation 4 is implicitly satisfied, spurious fluxes are avoided at the boundary between the atomistic and CG regimes. Each time a molecule crosses a boundary between the different regimes, it gains or loses on the fly (depending on whether it leaves or enters the CG region) its equilibrated rotational and vibrational DOFs (in the present example) while retaining its linear momentum (14, 64–66). This change in resolution requires the addition or removal of latent heat and thus must be accompanied with a thermostat that couples locally to the particle motion [e.g., Langevin or dissipative particle dynamics thermostats (67)].

One could also attempt to introduce a mixing scheme along the concept of Equation 7 directly on the interaction potentials rather than the forces (68). However, this leads to a violation of Newton's third law and consequently to nonconservation of the linear momentum (14, 62). Furthermore, in that case the total force not only would be the function of the gradients of the explicit and CG potentials, but would also depend linearly on the respective potentials themselves. Because these potentials are defined up to an arbitrary constant, that would lead to an arbitrary force component. The idea of decoupling DOFs rather than switching them on and off is attractive at first sight. Again this concept only works for DOFs that are eigenmodes of the molecules without any coupling to the surrounding (62). Because of these restrictions, we chose the above force interpolation scheme.

**Calculating average quantities in the transition regime: fractional calculus.** Introducing a thermostat requires a well-defined temperature. In regions $A$ and $B$ this is obvious; however, in the transition region $\Delta$, this is based on a generalization of

the equipartition theorem to the noninteger DOFs.[3] Let us assume that we want to switch on/off the DOF $q$ in the transition region $\Delta$ by a parameter $\alpha$. Then the equipartition theorem generalizes to

$$\langle K \rangle_\alpha = \frac{\alpha k_B T}{2}, \tag{8}$$

where $\langle K \rangle_\alpha$ is the average kinetic energy associated with the fractional DOF $q$, and $\alpha = w(x)$ is the level of resolution (14, 62). For more details on the required fractional calculus, we refer the reader to References 69–73. Equation 8 allows one to apply the usual thermostats, which are needed to supply or remove the latent heat when a molecule passes through the transition regime.



## 3.3. Applications

Thus far, we have applied the AdResS method presented in the section above to a liquid of nonpolar tetrahedral molecules, a generic solvated macromolecule, and liquid water (12, 13, 74, 75). We carried out all our hybrid multiscale simulations using a special modification of the ESPResSo package (76).

**Liquid of tetrahedral molecules.** The first test and proof of principle dealt with a liquid of simple model tetrahedral molecules (12) mentioned above. This model liquid mimics a typical liquid such as methane (68, 77). Each molecule in this system comprises four equal atoms with mass $m_0$. Their size $\sigma$ is fixed via the repulsive Weeks-Chandler-Andersen potential:

$$U^{ex}_{rep}(r_{i\alpha j\beta}) = \begin{cases} 4\varepsilon\left[\left(\frac{\sigma}{r_{i\alpha j\beta}}\right)^{12} - \left(\frac{\sigma}{r_{i\alpha j\beta}}\right)^{6} + \frac{1}{4}\right]; & r_{i\alpha j\beta} \le 2^{1/6}\sigma \\ 0; & r_{i\alpha j\beta} > 2^{1/6}\sigma \end{cases}, \tag{9}$$

where the cutoff at $2^{1/6}\sigma$, $\sigma$, and $\varepsilon$ are the standard Lennard-Jones parameters of length and energy, and $r_{i\alpha j\beta}$ is the distance between the atom $i$ of the molecule $\alpha$ and the atom $j$ of the molecule $\beta$. All atoms of a molecule $\alpha$ are connected by finitely extensible nonlinear elastic bonds:

$$U^{ex}_{bond}(r_{i\alpha j\alpha}) = \begin{cases} -\frac{1}{2}kR_0^2 \ln\left[1 - \left(\frac{r_{i\alpha j\alpha}}{R_0}\right)^2\right]; & r_{i\alpha j\alpha} \le R_0 \\ \infty; & r_{i\alpha j\alpha} > R_0 \end{cases}, \tag{10}$$

with $R_0 = 1.5\sigma$ and $k = 30\varepsilon/\sigma^2$. For technical details, we refer the reader to References 12 and 13.

In these tests we treat a medium-density liquid with a molecular number density of $\rho = 0.1/\sigma^3 \approx 0.57/\sigma_{cg}^3$ (12) and a high-density liquid with $\rho = 0.175/\sigma^3 \approx 1.0/\sigma_{cg}^3$ ($\sigma_{cg}$ is the excluded volume diameter of the CG molecule). Besides the slablike geometry, we also studied a spherical cavity-like geometry (13) (see **Figure 6*b***). The

[3] A fully switched-on DOF in the atomistic regime corresponds to $w = 1$, and a completely switched-off DOF in the CG regime corresponds to $w = 0$, whereas in the transition regime $\Delta$, where $0 \le w \le 1$, we deal with fractional DOFs, represented by their reduced phase space dimension.

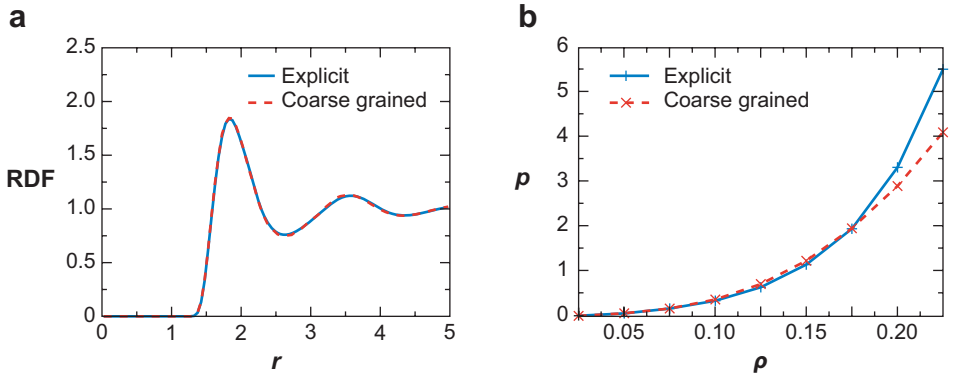


**Figure 7**

(*a*) The center-of-mass radial distribution function ($RDF_{cm}$) of the explicit and coarse-grained systems at $T = 1$ and $\rho = 0.175$. The two $RDF_{cm}$s match to the line thickness. (*b*) Equation of state for the explicit and coarse-grained systems at $T = 1$ and $\rho = 0.175$. Shown is the pressure $p$ as a function of the number density $\rho$ of the system. The equations of state coincide around the state points for which the effective potentials were parameterized. Figure adapted from Reference **13**.

latter example will be useful for studies of macromolecules embedded in a solvent, whereas the former can be readily extended to studies of liquids near (metal) surfaces (25, 32, 33, 78, 79). Below we use, if not specified otherwise, the dimensionless Lennard-Jones units (80).

To implicitly satisfy the boundary condition (4), we map the explicit atomistic (*ex*) model to a CG mesoscopic model. The latter comprises $N$ one-particle molecules as schematically depicted in **Figure 6*a***. A given CG molecule $\alpha$ in the system has a mass $M_\alpha = 4m_0$ equal to the total mass of the explicit tetrahedral molecule. All rotational and vibrational DOFs of atomistically resolved tetrahedral molecules are thus removed, and the number of nonbonded interactions is strongly decreased as well. We derive the effective density- and temperature-dependent CG potential $U^{cg}(r)$ in such a way that the center-of-mass radial distribution function ($RDF_{cm}$) (and thus the density) and pressure of the CG system match the corresponding $RDF_{cm}$ and pressure of the *ex* system at a given density and temperature (58).[4] For the effective pair potential derivation, one can resort to various methods found in the literature (e.g., see 16, 24, 61, 81). This means that at the chosen state point, the equations of state for the *ex* and CG systems coincide. The effective pair potential acting between the CG molecules is significantly softer than the pair potential between the atoms of the resolved molecules (12, 13) because it mimics a collection of atoms (e.g., see also 82, 83).

**Figure 7*a*,*b*** displays the $RDF_{cm}$s and equations of state for the *ex* and CG systems, respectively, which are run using the tabulated effective potential, parameterized for $\rho = 0.175$ (13).

[4]Note that matching the $g(r)$ is not needed for the concept itself; however, it is advantageous for practical applications, as shown below.

Next, we couple the atomistic and mesoscopic system using the AdResS method (Equation 7). For that purpose we introduce the weighting function $w(x)$ for the slablike geometry or $w(r)$ for the spherical cavity-like geometry. $w$ has the shape of a $\cos^2$ or $\sin^2$ function to smoothly interpolate between the regimes and to have zero slope at the boundaries $\pm d$ of the transition regime $\Delta$.

Within the transition regime, the pair force between the atoms $i\alpha$ and $j\beta$ of either explicit or hybrid molecules $\alpha$ and $\beta$, respectively, and the massless center of the molecule, which develops into the center of the CG particle, read as

$$\mathbf{F}_{i\alpha j\beta} = w(x_\alpha)w(x_\beta)\mathbf{F}^{ex}_{i\alpha j\beta} + [1 - w(x_\alpha)w(x_\beta)]\delta_{\alpha,\beta}\mathbf{F}^{ex}_{i\alpha j\beta} + [1 - w(x_\alpha)w(x_\beta)]\frac{m_{i\alpha}m_{j\beta}}{\sum_{i\alpha} m_{i\alpha} \sum_{j\beta} m_{j\beta}}\mathbf{F}^{cg}_{\alpha\beta}, \quad (11)$$

where $m_{i\alpha}$ and $m_{j\beta}$ are the masses of the respective atoms, and $\delta_{\alpha,\beta}$ is the Kronecker symbol. Summing over $i, j$ for $\alpha \neq \beta$ yields the total force $\mathbf{F}_{\alpha\beta}$ between molecules $\alpha$ and $\beta$ given in Equation 7.

To avoid any kinetic barrier for a free exchange of particles, the density profile should be totally flat, also throughout the transition regime. There is, however, no reason why any linear combination of two completely different sets of forces based on completely different interaction potentials should result in exactly the same pressure and density. Indeed the pressure in a system containing exclusively the hybrid molecules with constant $w \neq 0, 1$ slightly depends on the $w$ value (12). As it turns out, the pressure increase is most prominent for $w = 1/2$, which indicates that the most artificial case for the hybrid molecule is the mixture of one-fourth all-atom and three-fourths CG molecule. This justifies our asymmetric choice to use the switching factors $w(x_\alpha)w(x_\beta)$ and $1 - w(x_\alpha)w(x_\beta)$ in Equation 7, which are selected so that the worst case occurs precisely in the middle of the transition regime. In this way the all-atom and CG regimes are least affected.

To reduce density and pressure fluctuations, one can introduce a pressure correction function $s(w(R_\alpha)w(R_\beta))$ for the interpolation of the effective pair forces, $\mathbf{F}^{cg}_{\alpha\beta}$, between CG molecules (13). **Figure 8** displays the results of the density profile for a simple single-point version $s[x] = 4(\sqrt{x} - \frac{1}{2})^2$ of the interface pressure correction ($ex\text{-}cg_{ic}$). The correction involves a reparameterization of the effective pair potential in the system comprising exclusively hybrid molecules with the constant $w = 1/2$ over the whole system. In principle, one can arrive at a completely flat density profile by applying multiple point versions of $s$.

**Solvated macromolecule in a moving cell.** The next example generalizes our approach to the study of a polymer chain in solution (74) (**Figure 9**). The chain is surrounded by solvent with atomistic resolution. When the chain moves around, the sphere of atomistic resolution moves together with the center of mass of the chain. By this, the chain is free to move around, although the explicit resolution sphere is much smaller than the overall simulation volume. This enables us to efficiently treat solvation phenomena because only the solvent in the vicinity of a macromolecule is always represented with a sufficiently high level of detail so that the specific

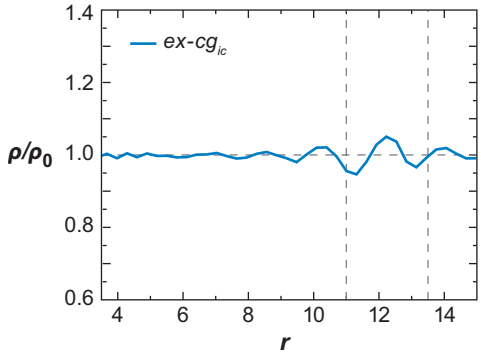


**Figure 8**

The normalized radial number density profiles of the *ex-cg*$_{ic}$ system at $\rho = 0.175$ and $T = 1$ for the radius of the explicit region $r_0 = 11.0$. Vertical lines denote boundaries between atomistic, coarse-grained, and interface regions of the system. Figure adapted from Reference 13.

interactions between a solvent and a solute are correctly taken into account. Solvent further away from the polymer, at which the high resolution is no longer required, is represented on a more CG level. In this work, a macromolecule is represented by a generic flexible polymer chain (84) embedded in a solvent of tetrahedral molecules introduced in the section above. To complete some of the first steps in the study of dynamics and to conserve momentum, we coupled the particle motion to the dissipative particle dynamics thermostat (67) instead of the Langevin thermostat employed

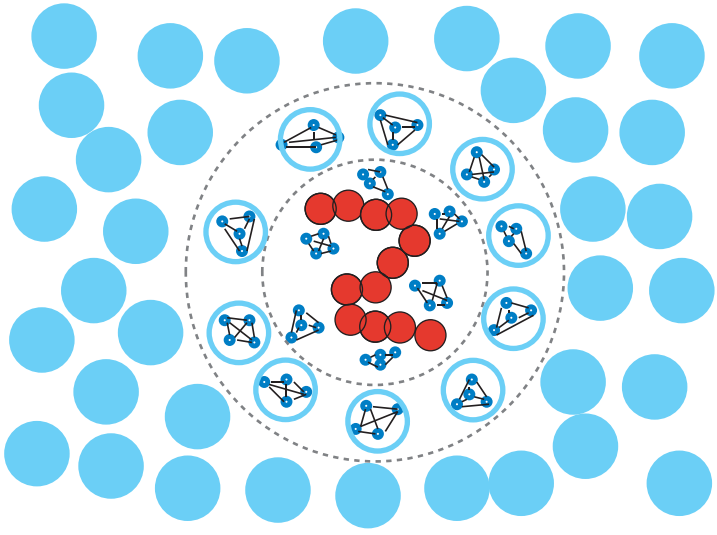

**Figure 9**

A schematic plot of a solvated generic bead-spring polymer. The polymer beads are represented smaller than the solvent molecules for clarity (for further details, see 74).

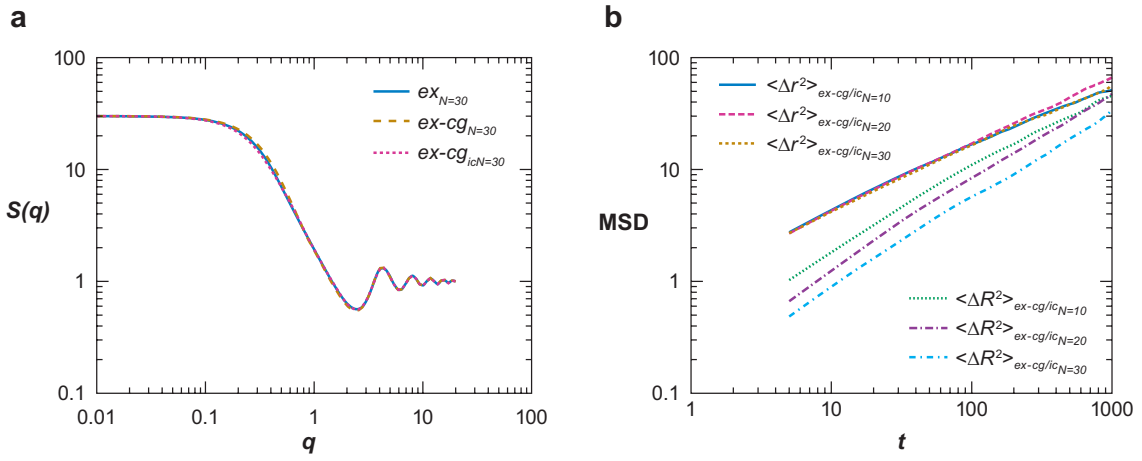


**Figure 10**

(*a*) The static structure factor of the polymer with $N = 30$ and a sphere radius of $r_0 = 12.0$ for the explicit (*ex*), explicit–coarse grained (*ex-cg*), and explicit–coarse grained with the interface pressure correction (*ex-cg*$_{ic}$) solvents. (*b*) Log-log plot of the time dependence of the mean square displacement (MSD) of a single monomer, $\langle \Delta r^2 \rangle$, for polymers and their centers of mass, $\langle \Delta R^2 \rangle$, with $N = 10$, 20, and 30 solvated in the hybrid *ex-cg*$_{ic}$ solvent. (We consider only monomers near the chain's center of mass.) Figure adapted from Reference 74.

in the other examples. With $\mathbf{R}_\alpha$, $\mathbf{R}_\beta$, and $\mathbf{R}$ as the centers of mass of the molecules $\alpha$, $\beta$, and the whole polymer, respectively, the AdResS method of Equation 7 is generalized to

$$\mathbf{F}_{\alpha\beta} = w(|\mathbf{R}_\alpha - \mathbf{R}|)w(|\mathbf{R}_\beta - \mathbf{R}|)\mathbf{F}^{ex}_{\alpha\beta} + [1 - w(|\mathbf{R}_\alpha - \mathbf{R}|)w(|\mathbf{R}_\beta - \mathbf{R}|)]\mathbf{F}^{cg}_{\alpha\beta} \qquad (12)$$

to account for the moving of the high-resolution scheme with the polymer. The size of the sphere is set such that the fluctuating polymer is always surrounded by the explicit solvent molecules. Thus Equation 12 for the forces in the transition regime only applies to the solvent.

**Figure 10*a*,*b*** compares the all-explicit simulation to the hybrid simulation scheme with and without the interface pressure correction applied in the transition regime. For the scattering function $S(q)$, the agreement is excellent, and even the mean square displacements of the beads are close to the expected power law of $t^{0.6}$, showing that the proposed scheme should at least be capable of properly reproducing the conformational statistics of the embedded polymer in solution. The resulting diffusion constants of the chains relate to the reduced viscosity of the CG liquid as we find, for example, $D(ex) = 0.0030$ compared with $D(ex\text{–}cg_{ic}) = 0.0035$. To improve this, we are currently testing new local thermostats for MD simulations (85).

**Liquid water.** In this section we extend our approach to polar liquids with long-range electrostatic interactions [i.e., the model of liquid water (75) depicted in **Figure 11**].

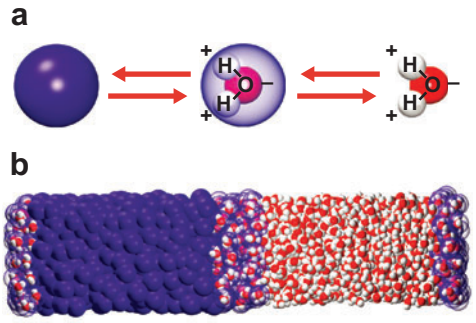


**Figure 11**

(*a*) On-the-fly interchange between the all-atom and coarse-grained water models. (*b*) A schematic representation of the hybrid liquid-water system.

We account for the long-range electrostatic interactions using the reaction field method, in which all molecules with the charge center outside a spherical cavity of a molecular-based cutoff radius $R_c = 9$ Å are treated as a dielectric continuum with a dielectric constant $\varepsilon_{RF}$ (86–89). The Coulomb force acting on a charge $e_{i\alpha}$, at the center of the cutoff sphere, due to a charge $e_{j\beta}$ within the cavity is

$$\mathbf{F}^{ex}_{C_{i\alpha j\beta}}(\mathbf{r}_{i\alpha j\beta}) = \frac{e_{i\alpha}e_{j\beta}}{4\pi\varepsilon_0}\left[\frac{1}{r^3_{i\alpha j\beta}} - \frac{1}{R_c^3}\frac{2(\varepsilon_{RF}-1)}{1+2\varepsilon_{RF}}\right]\mathbf{r}_{i\alpha j\beta}. \quad (13)$$

This allows us to introduce a new single-site water model in the CG regime, which contains no dipole moment. The single-site[5] water model (75) reproduces remarkably well the essential thermodynamic and structural features of water, as obtained by detailed all-atom simulations using the rigid TIP3P (90) water model. To derive the effective potential between CG molecules, we follow an iterative inverse statistical mechanics approach proposed by Lyubarstev & Laaksonen (91) (see **Figure 12**). A perfect agreement between the all-atom and CG $RDF_{cm}$s is reached using the optimized effective potential (shown in the inset of **Figure 12*a***). The effective potential has the first primary minimum at approximately 2.8 Å, corresponding to the first peak in the $RDF_{cm}$. The slightly weaker and significantly broader minimum at 4.5 Å corresponds to the second hydration shell. The combined effect of the two minima leads to a local packing close to that of the all-atom TIP3P water.

To more thoroughly quantify the structural properties of our model that are not completely defined by the RDF, we computed the distribution of the angle $\theta$ between the center of mass of three nearest-neighbor molecules and the orientational order parameter $q$ as defined by Errington & Debenedetti (92): $q = 1 - \frac{3}{8}\sum_{j=1}^{3}\sum_{k=j+1}^{4}(\cos\psi_{jk} + \frac{1}{3})^2$, where $\psi_{jk}$ is the angle formed by the lines

[5]The simulation speed up would be even larger if a CG spherical bead represented several water molecules, as is the case in dissipative particle dynamics simulations. However, because the lifetime of tetrahedral clusters is well below 1 ps in water, atomistic water molecules are not easily united into a CG bead. The water molecules could move apart in the transition regime, which would require the redistribution of the water molecules into CG beads on the fly. By mapping one atomistic water molecule to one CG bead, we avoid this problem.

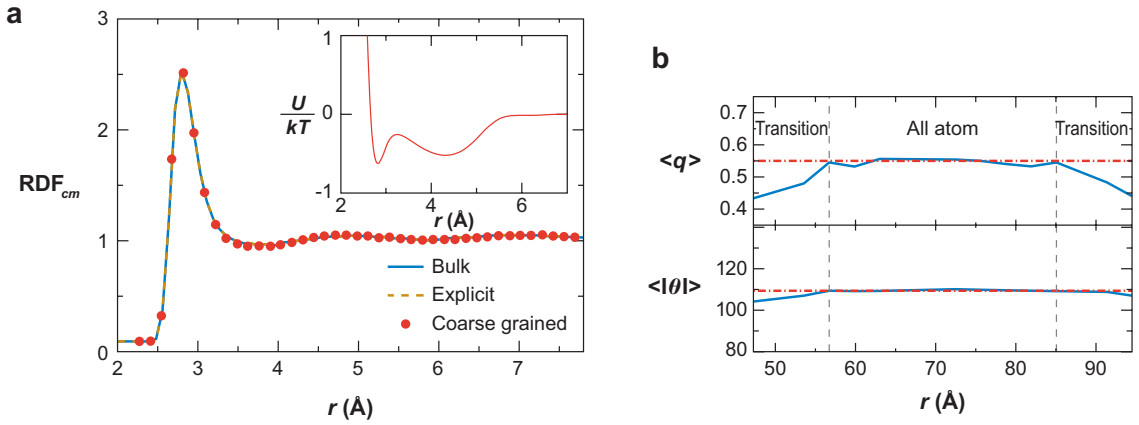


**Figure 12**

(*a*) The center-of-mass radial distribution functions (RDF$_{cm}$s) for explicit and coarse-grained regions of the hybrid system, together with the RDF$_{cm}$ corresponding to a bulk all-atom simulation. The local O-H and H-H RDFs for the explicit molecules in the hybrid system compare equally well to the standard bulk simulations (not shown). The optimized effective potential for the coarse-grained model is shown in the inset as a function of interparticle separation, *r*. (*b*, *top*) Average orientational order parameter *q* as a function of the coordinate *x* in the simulation box (all-atom and transition regime only). (*b*, *bottom*) Average center-of-mass angular distribution between three nearest neighbors as a function of the coordinate *x* in the simulation box. Figure adapted from Reference 75.

joining the oxygen atom of a given molecule and those of its nearest neighbors *j* and *k*. The parameter *q* measures the extent to which a molecule and its four nearest neighbors adopt a tetrahedral arrangement (92). Thus for a perfect tetrahedral network, $q = 1$, whereas for the random arrangement of molecules as in an ideal gas, $q = 0$. We find $\langle|\theta|_{ex}\rangle = 109.7 \pm 24.6$ and $\langle q\rangle_{ex} = 0.54 \pm 0.2$ for the explicit regime, and $\langle|\theta|_{cg}\rangle = 103.4 \pm 30.7$ and $\langle q\rangle_{cg} = 0.42 \pm 0.2$ for the CG regime. The reference bulk values are $\langle|\theta|_{bulk}\rangle = 109.4 \pm 24.6$ and $\langle q\rangle_{bulk} = 0.55 \pm 0.2$. Most importantly, the somewhat weak order of the CG water does not influence the structure in the all-atom regime as **Figure 12*b*** clearly shows.

From the data it is also evident that the structure in the atomistic region of the hybrid system is the same as in the bulk water. The normalized density for the hybrid system is homogeneous in the CG and explicit regions with (very) small oscillations in the transition regime (see **Figure 13**). To demonstrate the free exchange of molecules between the different regimes, we have computed the time evolution of a diffusion profile for molecules that were initially localized at the interface layer. **Figure 13** shows that these molecules spread out asymmetrically with time. This asymmetry arises from the aforementioned difference in diffusion coefficient between the all-atom and CG regions. However, this difference in time scale can even be advantageous for reaching longer effective simulation times in systems in which multiple length and time scales are intrinsically present. Along these lines AdResS can be applied to any

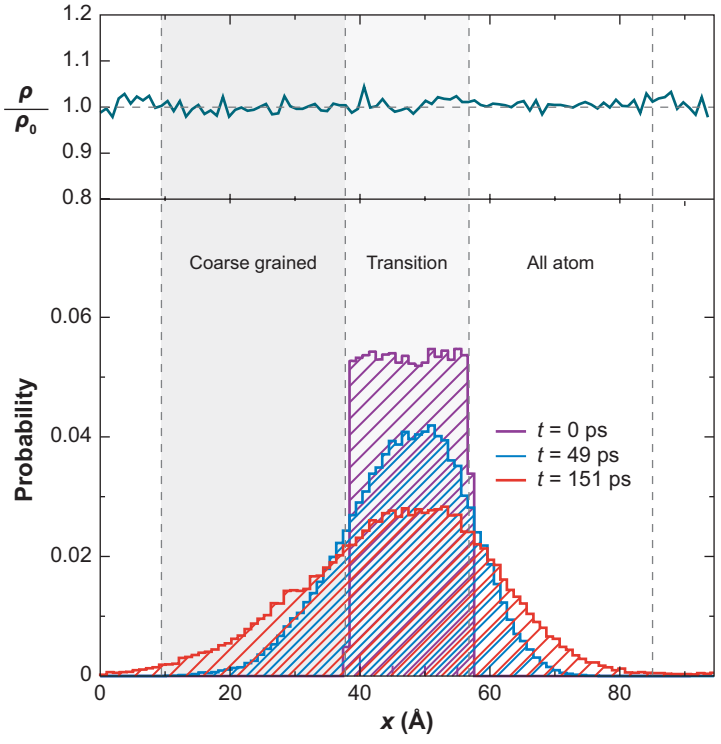


**Figure 13**

(*Top panel*) Normalized density profile in the $x$ direction of the hybrid system. (*Bottom panel*) Time evolution of a diffusion profile for the molecules that are initially (at time $t = 0$ ps) located in the interface region. The diffusion profile is averaged over ≈400 different time origins. Vertical lines denote the boundaries of the interface layer. Figure taken from Reference 75.

other flexible or rigid nonpolarizable classical water model (e.g., SPC, SPC/E, or TIP4P) (89, 93–96).

## 4. OUTLOOK

Many interesting problems in condensed matter are inherently multiscale, and it is exactly this scale interplay that drives the relevant properties of the system. Although analytic theory here can only be approximative, computer simulation can address this issue via time- and length-scale-bridging techniques. Quantum-classical atomistic and CG scales can be linked in a consistent sequential way to account for the different levels of detail and to reduce the computational effort massively. The example of bisphenol-A polycarbonate in bulk and at a metal surface illustrates the situation in its full meaning. It represents a typical case of coupling specific interactions at the surface (quantum scale) and global conformations (classical atomistic CG level).

However, it is exactly problems such as this that require new computational schemes that can account simultaneously for all relevant scales involved.

Specifically, the question arises as to whether one can devise an adaptive resolution method that allows the treatment of different regions with different resolutions, while allowing the free exchange of particles among such regions. For a macromolecule-surface system, this translates into the possibility of having the specific atomistic interactions between the surface and polymer at the very surface and far from the surface in only a CG model. As a bead approaches the surface, it slowly acquires the atomistic structure (and loses the CG one), whereas it does the opposite when moving away from the surface. The answer to this question is represented by the AdResS method, discussed above. This method allows us to change DOFs on the fly during a simulation run and thus allows us to adaptively change the molecule's resolution in a given region of space while keeping the free exchange of molecules among the regions of different resolution. So far this method has been applied to a liquid of tetrahedral molecules, the solvation of a bead-spring model of polymer in a solvent comprising tetrahedral molecules, and finally liquid water. These systems are technical prototypes for further realistic applications such as the solvation of large molecules and surface-polymer systems.

All these approaches bear some, although limited, analogy to critical phenomena and renormalization group theory. Along these lines, it is highly desirable (next to the quantitative description of material and system properties, of course) to learn more about how specific local interactions translate or do not translate into macroscopic structures and properties.

## SUMMARY POINTS

1. The multiscale modeling of soft matter attempts to link the relevant length scales that determine the macroscopic properties of a material in a systematic way. This is especially relevant for soft matter because properties on an angstrom scale link to conformational and composition fluctuations on the nanometer and micrometer scale and in addition cover many decades in time.
2. Structure-based coarse graining is a variant of multiscale modeling that treats bonded and nonbonded interactions separately. We discuss above an example in which a close link of the CG model to the chemical structure is maintained. Because the overall structural properties on different resolution levels are conserved, a systematic scale hopping between different levels is possible. This approach also allows one to efficiently study the dynamics of polymeric systems.
3. Dual-scale modeling is an extension of structure-based coarse graining for the case in which a higher resolution is needed at certain positions within a macromolecule. Above we apply this to the angular resolution at the terminal groups of bisphenol-A polycarbonate, when they approach a metal surface.

4. AdResS allows one to study a given system on different resolution levels within one simulation. Absolutely necessary for the application of soft matter problems is the free exchange of particles between the different regimes. By this there is also the option to have the region of high resolution move with a molecule or adjust it locally at will. To link the different resolution levels in one simulation, we had to extend the equipartition theorem to fractional DOFs to define a temperature and thus a thermostat in the transition regime.

## DISCLOSURE STATEMENT

The authors are not aware of any biases that might be perceived as affecting the objectivity of this review.

## ACKNOWLEDGMENTS

Over the years we have collaborated with many colleagues and students on the topics described in this review. We would like to especially thank C.F. Abrams, S. Leon, F. Müller-Plathe, N. van der Vegt, C. Peter, B. Hess, V. Harmandaris, C. Clementi, S. Matysiak, and the ESPResSo team for fruitful collaboration and many discussions. This research in part was supported within the BMBF Center on Multiscale Materials Simulations, the Volkswagen Foundation, and the Bayer AG and BASF AG.

## LITERATURE CITED

1. Flory PJ. 1953. *Principles of Polymer Chemistry*. Ithaca, NY: Cornell Univ. Press
2. Flory PJ. 1969. *Statistical Mechanics of Chain Molecules*. New York: Interscience
3. de Gennes PG. 1979. *Scaling Concept in Polymer Physics*. Ithaca, NY: Cornell Univ. Press
4. Doi M, Edwards SF. 1986. *The Theory of Polymer Dynamics*. Oxford: Clarendon
5. Binder K, ed. 1995. *Monte Carlo and Molecular Dynamics Simulation in Polymer Science*. Oxford: Clarendon
6. **Tschöp W, Kremer K, Batoulis J, Bürger T, Hahn O. 1998. Simulation of polymer melts. I. Coarse-graining procedure for polycarbonates. *Acta Polym.* 49:61–74**
7. Tschöp W, Kremer K, Hahn O, Batoulis J, Bürger T. 1998. Simulation of polymer melts. II. From coarse-grained models back to atomistic description. *Acta Polym.* 49:75–79
8. Kremer K. 2000. Computer simulations in soft matter science. In *Soft and Fragile Matter, Nonequilibrium Dynamics, Metastability and Flow, Proc. NATO ASI*

**6. Along with Ref. 7, first structure-based coarse-graining simulation, including the backmapping and separation of bonded and nonbonded interactions.**

*Workshop, St. Andrews, Summer 1999*, ed. ME Cates, MR Evans, pp. 145–84. Bristol: Inst. Phys.

**9. Eilhard J, Zirkel A, Tschöp W, Hahn O, Kremer K, et al. 1999. Spatial correlations in polycarbonates: neutron scattering and simulation. *J. Chem. Phys.* 110:1819–30**

**10. Abrams CF, Kremer K. 2003. Combined coarse-grained and atomistic simulation of liquid bisphenol-A-polycarbonate: liquid packing and intramolecular structure. *Macromolecules* 36:260–67**

11. van der Vegt NFA, Peter C, Kremer K. 2008. Structure-based coarse- and fine-graining in soft matter simulations. In *Coarse-Graining of Condensed Phase and Biomolecular Systems*, ed. GA Voth. Boca Raton, FL: Chapman & Hall/CRC. In press

**12. Praprotnik M, Delle Site L, Kremer K. 2005. Adaptive resolution molecular dynamics simulation: changing the degrees of freedom on the fly. *J. Chem. Phys.* 123:224106**

13. Praprotnik M, Delle Site L, Kremer K. 2006. Adaptive resolution scheme (AdResS) for efficient hybrid atomistic/mesoscale molecular dynamics simulations of dense liquids. *Phys. Rev. E* 73:066701

**14. Praprotnik M, Kremer K, Delle Site L. 2007. Adaptive molecular resolution via a continuous change of the phase space dimensionality. *Phys. Rev. E* 75:017701**

15. Baschnagel J, Binder K, Doruker P, Gusev AA, Hahn O, et al. 2000. Bridging the gap between atomistic and coarse-grained models of polymers: status and perspectives. *Adv. Polym. Sci.* 152:41–156

16. Reith D, Pütz M, Müller-Plathe F. 2003. Deriving effective mesoscale potentials from atomistic simulations. *J. Comput. Chem.* 24:1624–36

17. Müller-Plathe F. 2003. Scale-hopping in computer simulations of polymers. *Soft Mater.* 1:1–31

**18. Murat M, Kremer K. 1998. From many monomers to many polymers: soft elliptoid model for polymer melts and mixtures. *J. Chem. Phys.* 108:4340–48**

19. Eurich F, Maass P. 2001. Soft ellipsoid model for Gaussian polymer chains. *J. Chem. Phys.* 114:7655–68

20. Louis AA, Bolhuis PG, Hansen JP, Meijer EJ. 2000. Can polymer coils be modeled as 'soft colloids'? *Phys. Rev. Lett.* 85:2522–25

21. Ferraio M, Ciccotti G, Binder K, eds. 2006. *Computer Simulations in Condensed Matter Systems: From Materials to Chemical Biology*, Vol 1. Lect. Notes Phys. Berlin: Springer

22. Ferraio M, Ciccotti G, Binder K, eds. 2006. *Computer Simulations in Condensed Matter Systems: From Materials to Chemical Biology*, Vol. 2. Lect. Notes Phys. Berlin: Springer

23. Harmandaris V, Reith D, van der Vegt NF, Kremer K. 2007. Comparison between coarse-graining models for polymers systems: two mapping schemes for polystyrene. *Macromol. Chem. Phys.* 208:2109–20

**9. Detailed comparison of simulations of different polycarbonate modifications to neutron scattering of protonated and deuterated samples.**

**10. Detailed comparison of two closely related coarse-graining schemes for polycarbonate, showing that a coarser structure can also be less efficient.**

**12. Introduces the first adaptive resolution simulation (AdResS) for a liquid of simple tetrahedral molecules.**

**14. Along with Ref. 62, generalizes the equipartition theorem for fractional DOFs, which allows the definition of a temperature and the construction of a thermostat in the transition regime.**

**18. Maps a whole polymer chain onto one soft ellipsoid and tests for simple model polymer mixtures.**

24. Lyubartsev AP, Laaksonen A. 1995. Calculation of effective interaction potentials from radial distribution functions: a reverse Monte Carlo approach. *Phys. Rev. E* 52:3730–37
25. Abrams CF, Delle Site L, Kremer K. 2003. Dual-resolution coarse-grained simulation of the bisphenol-A-polycarbonate/nickel interface. *Phys. Rev. E* 67:021807
26. Auhl R, Everaers R, Grest GS, Kremer K, Plimpton SJ. 2003. Equilibration of long chain polymer melts in computer simulations. *J. Chem. Phys.* 119:12718–28
**27. Leon S, Delle Site L, van der Vegt NFA, Kremer K. 2005. Bisphenol-A polycarbonate: entanglement analysis from coarse-grained MD simulations. *Macromolecules* 38:8078–92**
28. Hess B, Leon S, van der Vegt N, Kremer K. 2006. Long time atomistic polymer trajectories from coarse grained simulations: bisphenol-A polycarbonate. *Soft Matter* 2:409–14
29. Heath AP, Kavraki LE, Clementi C. 2007. From coarse-grain to all-atom: toward multiscale analysis of protein landscapes. *Proteins* 68:646–61
**30. Hahn O, Mooney DA, Müller-Plathe F, Kremer K. 1999. A new mechanism for penetrant diffusion in amorphous polymers: molecular dynamics simulations of phenol diffusion in bisphenol-A-polycarbonate. *J. Chem. Phys.* 111:6061–68.**
31. Harmandaris VA, Adhikari NP, van der Vegt NFA, Kremer K. 2006. Hierarhical modeling of polystyrene: from atomistic to coarse-grained simulations. *Macromolecules* 39:6708–19
**32. Delle Site L, Abrams CF, Alavi A, Kremer K. 2002. Polymers near metal surfaces: selective adsorption and global conformations. *Phys. Rev. Lett.* 89:156103**
33. Delle Site L, Leon S, Kremer K. 2004. BPA-PC on a Ni(111) surface: the interplay between adsorption energy and conformational entropy for different chain-end modifications. *J. Am. Chem. Soc.* 126:2944–55
34. Zhou X, Andrienko D, Delle Site L, Kremer K. 2005. Dynamics surface decoupling in a sheared polymer melt. *Europhys. Lett.* 70:264–70
35. Zhou X, Andrienko D, Delle Site L, Kremer K. 2005. Flow boundary conditions for chain-end adsorbing polymer melts. *J. Chem. Phys.* 123:104904
36. Andrienko D, Leon S, Delle Site L, Kremer K. 2005. Adhesion of polycarbonate blends on a nickel surface. *Macromolecules* 38:5810–16
37. Delle Site L, Leon S, Kremer K. 2005. Specific interaction of polymers with surface defects: structure formation of polycarbonate on nickel. *J. Phys. Condens. Matter* 17:L53–60
38. Villa E, Balaeff A, Mahadevan L, Schulten K. 2004. Multiscale method for simulating protein-DNA complexes. *Multiscale Model. Simul.* 2:527–53
39. Neri M, Anselmi C, Cascella M, Maritan A, Carloni P. 2005. Coarse-grained model of proteins incorporating atomistic detail of the active site. *Phys. Rev. Lett.* 95:218102
40. Rafii-Tabar H, Hua L, Cross M. 1998. A multi-scale atomistic-continuum modelling of crack propagation in a two-dimensional macroscopic plate. *J. Phys. Condens. Matter* 10:2375–87

**27. Along with Ref. 28, detailed analysis of the dynamics of polycarbonates; remapping of details yields atomistic trajectories of highly entangled polymers for more than $10^{-5}$ s.**

**30. Using remapped polycarbonate melts as a matrix for studies of the diffusion of phenol, reveals a phenol-polymer correlated hopping diffusion mechanism.**

**32. Along with Ref. 33, treats selective adsorption of polycarbonate chain ends as a function different chain ends, based on a combination of Car-Parrinello MD calculations and coarse-grained simulation.**

41. Broughton JQ, Abraham FF, Bernstein N, Kaxiras E. 1999. Concurrent coupling of length scales: methodology and application. *Phys. Rev. B* 60:2391–403
42. Smirnova JA, Zhigilei LV, Garrison BJ. 1999. A combined molecular dynamics and finite element method technique applied to laser induced pressure wave propagation. *Comp. Phys. Commun.* 118:11–16
43. Csanyi G, Albaret T, Payne MC, DeVita A. 2004. 'Learn on the fly': a hybrid classical and quantum-mechanical molecular dynamics simulation. *Phys. Rev. Lett.* 93:175503
44. O'Connell ST, Thompson PA. 1995. Molecular dynamics–continuum hybrid computations: a tool for studying complex fluid flows. *Phys. Rev. E* 52:R5792–95
45. Hadjiconstantinou NG. 1999. Combining atomistic and continuum simulations of contact-line motion. *Phys. Rev. E* 59:2475–78
46. Li J, Liao D, Yip S. 1998. Coupling continuum to molecular-dynamics simulation: reflecting particle method and the field estimator. *Phys. Rev. E* 57:7259–67
47. Flekkoy EG, Wagner G, Feder J. 2000. Hybrid model for combined particle and continuum dynamics. *Europhys. Lett.* 52:271–76
48. Delgado-Buscalioni R, Coveney PV. 2003. Continuum-particle hybrid coupling for mass, momentum, and energy transfers in unsteady fluid flow. *Phys. Rev. E* 67:046704
49. Koumoutsakos P. 2005. Multiscale flow simulations using particles. *Annu. Rev. Fluid Mech.* 37:457–87
50. Lyman E, Ytreberg FM, Zuckerman DM. 2006. Resolution exchange simulation. *Phys. Rev. Lett.* 96:028105
51. Backer JA, Lowe CP, Hoefsloot HCJ, Ledema PD. 2005. Combined length scales in dissipative particle dynamics. *J. Chem. Phys.* 123:114905
52. Christen M, van Gunsteren WF. 2006. Multigraining: an algorithm for simultaneous fine-grained and coarse-grained simulation of molecular systems. *J. Chem. Phys.* 124:154106
53. Fabritiis GD, Delgado-Buscalioni R, Coveney PV. 2006. Multiscale modeling of liquids with molecular specificity. *Phys. Rev. Lett.* 97:134501
54. Curtarolo S, Ceder G. 2002. Dynamics of an inhomogeneously coarse grained multiscale system. *Phys. Rev. Lett.* 88:255504
55. Chun HM, Padilla CE, Chin DN, Watanabe M, Karlov VI, et al. 2000. MBO(N)D: a multibody method for long-time molecular dynamics simulations. *J. Comput. Chem.* 21:159–84
56. Malevanets A, Kapral R. 2000. Solute molecular dynamics in a mesoscale solvent. *J. Chem. Phys.* 112:7260–69
57. Laio A, VandeVondele J, Röthlisberger U. 2002. A Hamiltonian electrostatic coupling scheme for hybrid Car-Parrinello molecular dynamics simulations. *J. Chem. Phys.* 116:6941
58. Henderson RL. 1974. A uniqueness theorem for fluid pair correlation functions. *Phys. Lett.* 49:A197–98
59. Soper AK. 1996. Empirical Monte Carlo simulation of fluid structure. *Chem. Phys.* 202:295–306

60. Izvekov S, Parrinello M, Burnham CB, Voth GA. 2004. Effective force fields for condensed phase systems from ab initio molecular dynamics simulation: a new method for force matching. *J. Chem. Phys.* 120:10896–913
61. Izvekov S, Voth GA. 2005. Multiscale coarse graining of liquid-state systems. *J. Chem. Phys.* 123:134105
62. Praprotnik M, Kremer K, Delle Site L. 2007. Fractional dimensions of phase space variables: a tool for varying the degrees of freedom of a system in a multiscale treatment. *J. Phys. A Math. Theor.* 40:F281–88
63. Goldstein H. 1980. *Classical Mechanics*. Reading, MA: Addison-Wesley. 2nd ed.
64. Janežič D, Praprotnik M, Merzel F. 2005. Molecular dynamics integration and molecular vibrational theory: I. New symplectic integrators. *J. Chem. Phys.* 122:174101
65. Praprotnik M, Janežič D. 2005. Molecular dynamics integration and molecular vibrational theory: II. Simulation of nonlinear molecules. *J. Chem. Phys.* 122:174102
66. Praprotnik M, Janežič D. 2005. Molecular dynamics integration and molecular vibrational theory: III. The infrared spectrum of water. *J. Chem. Phys.* 122:174103
67. Soddemann T, Dünweg B, Kremer K. 2003. Dissipative particle dynamics: a useful thermostat for equilibrium and nonequilibrium molecular dynamics simulations. *Phys. Rev. E* 68:046702
68. Ensing B, Nielsen SO, Moore PB, Klein ML, Parrinello M. 2007. Energy conservation in adaptive hybrid atomistic/coarse-grain molecular dynamics. *J. Chem. Theory Comput.* 3:1100–5
69. Nonnenmacher TF. 1990. Fractional integral and differential equations for a class of Levi-type probability densities. *J. Phys. A Math. Gen.* 23:LS697–700
70. Hilfer R, ed. 2000. *Applications of Fractional Calculus in Physics*. Singapore: World Sci.
71. Cotrill-Shepherd K, Naber M. 2001. Fractional differential forms. *J. Math. Phys.* 42:2203–12
72. Tarasov VE. 2004. Fractional generalization of Liouville equations. *Chaos* 14:123–27
73. Tarasov VE. 2005. Fractional systems and fractional Bogoliubov hiearchy equations. *Phys. Rev. E* 71:011102
74. Praprotnik M, Delle Site L, Kremer K. 2007. A macromolecule in a solvent: adaptive resolution molecular dynamics simulation. *J. Chem. Phys.* 126:134902
**75. Praprotnik M, Matysiak S, Delle Site L, Kremer K, Clementi C. 2007. Adaptive resolution simulation of liquid water. *J. Phys. Condens. Matter* 19:292201**
76. Limbach HJ, Arnold A, Mann BA, Holm C. 2006. ESPResSo: an extensible simulation package for research on soft matter systems. *Comp. Phys. Comm.* 174:704–27
77. Abrams CF. 2005. Concurrent dual-resolution Monte Carlo simulation of liquid methane. *J. Chem. Phys.* 123:234101
78. Schravendijk P, van der Vegt N, Delle Site L, Kremer K. 2005. Dual scale modeling of benzene adsorption onto Ni(111) and Au(111) surfaces in explicit water. *Chem. Phys. Chem.* 6:1866–71

**75. First application and test of the new AdResS simulation ansatz to liquid water.**

79. Nielsen SO, Srinivas G, Klein ML. 2005. Incorporating a hydrophobic solid into a coarse grain liquid framework: graphite in an aqueous amphiphilic environment. *J. Chem. Phys.* 123:124907
80. Allen MP, Tildesley DJ. 1987. *Computer Simulation of Liquids*. Oxford: Clarendon
81. Müller-Plathe F. 2002. Coarse-graining in polymer simulation: from the atomistic to the mesoscopic scale and back. *Chem. Phys. Chem.* 3:754–69
82. Klapp SHL, Diestler DJ, Schoen M. 2004. Why are effective potentials 'soft'? *J. Phys. Condens. Matter* 16:7331–52
83. Bryant G, Williams SR, Qian L, Snook IK, Perez E, Pincet F. 2002. How hard is a colloidal 'hard-sphere' interaction? *Phys. Rev. E* 66:060501
84. Kremer K, Grest GS. 1990. Dynamics of entagled linear polymer melts: a molecular-dynamics simulation. *J. Chem. Phys.* 92:5057–86
85. Junghans C, Praprotnik M, Kremer K. 2008. Transport properties controlled by a thermostat: an extended dissipative particle dynamics thermostat. *Soft Matter* 4:156–61
86. Neumann M. 1983. Dipole moment fluctuation formulas in computer simulations of polar systems. *Mol. Phys.* 50:841–58
87. Neumann M. 1985. The dielectric constant of water: computer simulations with the MCY potential. *J. Chem. Phys.* 82:5663–72
88. Tironi IG, Sperb R, Smith PE, van Gunsteren WF. 1995. A generalized reaction field method for molecular dynamics simulations. *J. Chem. Phys.* 102:5451–59
89. Praprotnik M, Janežič D, Mavri J. 2004. Temperature dependence of water vibrational spectrum: a molecular dynamics simulation study. *J. Phys. Chem. A* 108:11056–62
90. Jorgensen WL, Chandrasekhar J, Madura JD, Impey RW, Klein ML. 1983. Comparison of simple potential functions for simulating liquid water. *J. Chem. Phys.* 79:926–36
91. Lyubartsev AP, Laaksonen A. 1995. Calculations of effective interactions potentials from radial distribution functions: a reverse Monte Carlo approach. *Phys. Rev. E* 52:3730–37
92. Errington JR, Debenedetti PG. 2001. Relationship between structural order and the anomalies of liquid water. *Nature* 409:318–21
93. Berendsen HJC, Postma JPM, van Gunsteren WF, Hermans J. 1981. Molecular dynamics simulations: the limits and beyond. In *Intermolecular Forces*, ed. B Pullman, pp. 331–42. Dordrecht: Reidel
94. Berendsen HJC, Grigera JR, Straatsma TP. 1987. The missing term in effective pair potentials. *J. Phys. Chem.* 91:6269–71
95. Lawrence CP, Skinner JL. 2003. Flexible TIP4P model for molecular dynamics simulation of liquid water. *Chem. Phys. Lett.* 372:842–47
96. Johnson ME, Head-Gordon T, Louis AA. 2007. Representability problems for coarse-grained water potentials. *J. Chem. Phys.* 126:144509

Annual Review of
Physical Chemistry

Volume 59, 2008

# Contents

**Indexes**



**Errata**

An online log of corrections to *Annual Review of Physical Chemistry* articles may be found at http://physchem.annualreviews.org/errata.shtml